Journal of Inorganic and General Chemistry
ZAAC
Zeitschrift für anorganische und allgemeine Chemie

DOI: 10.1002/zaac.201800332

ARTICLE

Synthesis, Crystal Structures, and Properties of Ni(NCS)$_2$-4-methoxypyridine Coordination Compounds

Aleksej Jochim,[a] Magdalena Ceglarska,[b] Michał Rams,[b] and Christian Näther*[a]

Dedicated to Prof. Dr. Wolfgang Bensch on the Occasion of his 65th Birthday

Abstract. Two polymorphs of Ni(NCS)$_2$(4-methoxypyridine)$_4$ (**1-I**, **1-II**) as well as compounds with the compositions Ni(NCS)$_2$(4-methoxypyridine)$_4$(MeCN)$_{1.33}$ (**1-MeCN**), Ni(NCS)$_2$(4-methoxypyridine)$_2$(MeCN)$_2$ (**2**) and [Ni(NCS)$_2$(4-methoxypyridine)$_2$]$_n$ (**3**) are reported. For **1-II** no single crystals were obtained, but this compound is isotypic to the Fe analog **1-II-Fe**. The crystal structures of **1** and **2** show discrete octahedral Ni^{II} complexes, whereas in **3** the cations are connected by pairs of thiocyanate anions into chains. Solvent mediated conversion experiments reveal that **1-I** is thermodynamically stable at room temperature and differential scanning calorimetry shows no indication for a polymorphic transition. The thermal behavior of **1-I**, **1-II**, and **2** was investigated by simultaneous thermogravimetry and differential scanning calorimetry, which shows that they decompose in two discrete steps. In the first step compound **3** is formed as an intermediate, which decomposes on further heating into Ni(NCS)$_2$. Time dependent XRPD investigations prove, that **2** transforms already at room temperature into **3**. Upon heating **1-MeCN** transforms into **1-I** in the first TG step, which decomposes on further heating into **3**. Investigation of the magnetic behavior of **3** shows dominating ferromagnetic exchange interactions along the chains with $J = 5.9(1)$ K. Susceptibility measurements indicate antiferromagnetic ordering, which was confirmed by specific heat measurements, revealing that magnetic ordering occurs at 1.91(5) K.

Introduction

The synthesis of new magnetic coordination compounds is still an important topic in modern coordination chemistry and an extremely large number of compounds showing a variety of magnetic properties has been reported.[1–10] In this regard one-dimensional coordination polymers, for which the magnetic properties largely depend on the strength of the exchange along the chains are of special interest.[11–17] This interaction is predominantly determined by the bridging ligand that mediates the magnetic exchange and therefore, replacement of one ligand by a different one is one possibility to influence the magnetic properties of such compounds in a desired way.

In this context numerous coordination polymers based on, e.g. transition metal cyanides or azides have been reported.[17–29] Compared to these, less compounds based on thio- or selenocyanate anions are known, which was one of the reasons why we became interested in this class of compounds several years ago.[30–36] While the magnetic exchange in compounds containing these anionic ligands is usually weaker than that in azides they show a larger structural diversity because of many different coordination modes of these anionic ligands.[31,37–48] Unfortunately for less chalcophilic metal cations, the coordination to the N atom is preferred and therefore, in most of them the anions are only terminally N-coordinated. Consequently the compounds with μ-1,3-bridging anions are usually more difficult to prepare and therefore, some time ago, we have reported an alternative approach that is based on thermal decomposition of suitable precursor compounds, in which the anionic ligands are only terminally coordinated.[46,49] Upon heating, the neutral co-ligands are usually removed stepwise, which enforces the formation of the desired compounds with bridging anionic ligands and in several cases metastable polymorphic modifications or different isomers can be obtained, which cannot be synthesized or that are at least difficult to prepare from solution.[45,49–52] Therefore, we are generally interested in the thermal properties of this class of compounds.

If the precursors consist of discrete complexes with pyridine derivatives as co-ligands, usually 1D compounds are obtained, in which the metal cations are octahedrally coordinated by two N-donor co-ligands as well as four μ-1,3-bridging anionic ligands and are linked by pairs of anionic ligands into chains[51,53–55] although examples of 2D networks are also known.[51,56–58] The 1D compounds with Co^{II} are of special interest, because the magnetic exchange along the chain is ferromagnetic and several of these coordination polymers show single chain magnetism.[54,55,59] For such compounds the magnetic properties largely depend on the strength of the magnetic exchange and therefore, we became generally interested in the relation between chain structure and chemical composition as well as the strength of the magnetic exchange. In this context

---

* Prof. Dr. C. Näther
E-Mail: cnaether@ac.uni-kiel.de
[a] Institute of Inorganic Chemistry
Christian-Albrechts-University of Kiel
Max-Eyth-Straße 2
24118 Kiel, Germany
[b] Institute of Physics
Jagiellonian University
Łojasiewicza 11
30348 Kraków, Poland

Supporting information for this article is available on the WWW under **http://dx.doi.org/10.1002/zaac.201800332** or from the author.

it is noted that the corresponding compounds with Ni^{II} show a similar structural behavior and are in several cases isotypic to its Co^{II} counterparts. Moreover, in these compounds the exchange along the chain is also ferromagnetic and in contrast to the Co^{II} compounds models are available, which can be used to extract the magnetic exchange constant *J* for all kinds of chain structures. This is crucial, because dependent on the co-ligand these compounds can show a different chain arrangement and a different metal coordination.

As mentioned above, most compounds consist of linear chains, in which the thiocyanate N and S atoms as well as the co-ligand N atoms are in *trans* position. In the course of our systematic work we also prepared an isomer, in which the thiocyanate N and the thiocyanate S atoms are *cis*, while the co-ligand is still *trans*, which also leads to the formation of linear chains.[60] Dependent on the co-ligand additional isomers were obtained, which also show a *cis-cis-trans* coordination or an alternating all-*trans* and *cis-cis-trans* coordination but in this case the thiocyanate N atoms are *cis*, leading to the formation of corrugated chains.[61]

For these compounds the magnetic exchange constant *J* was extracted from magnetic measurements, which indicate that the magnetic exchange in corrugated chains is lower than in linear chains. Unfortunately, no simple rules can be extracted regarding the influence of geometrical parameters like distances and angles or the nature of the co-ligand on *J*, which indicates that even small variations have a large impact on the magnetic exchange. This might be traced back to the relatively low data basis, because for these isomers only a limited number of examples are available. All this is the reason why we are still interested in the syntheses, crystal structures, and magnetic properties of such Ni^{II} chain compounds and in the course of this project we selected 4-methoxypyridine as co-ligand, which exhibits a strong donor substituent in 4-position. In this context it would be of interest, which chain isomer is obtained and which value for the magnetic exchange constant can be found. We also tried to prepare precursor complexes, which on thermal decomposition might transform into different isomers, as recently observed for other compounds.[45,51] Herein we report on our investigations.

Results and Discussion

Synthesis and Characterization

The reactions of $Ni(NCS)_2$ with 4-methoxypyridine in different molar ratios and solvents lead to the formation of three different crystalline compounds with the composition $Ni(NCS)_2$(4-methoxypyridine)$_4$ (**1-I**), $Ni(NCS)_2$(4-methoxypyridine)$_2$(MeCN)$_2$ (**2**), and $[Ni(NCS)_2(\text{4-methoxypyridine})_2]_n$ (**3**). Time dependant studies revealed that another compound could be obtained under kinetic control. This crystalline phase (**1-II**) has the same composition as **1-I**, but its powder diffraction pattern is completely different, indicating the formation of a polymorphic modification (Figure 1).

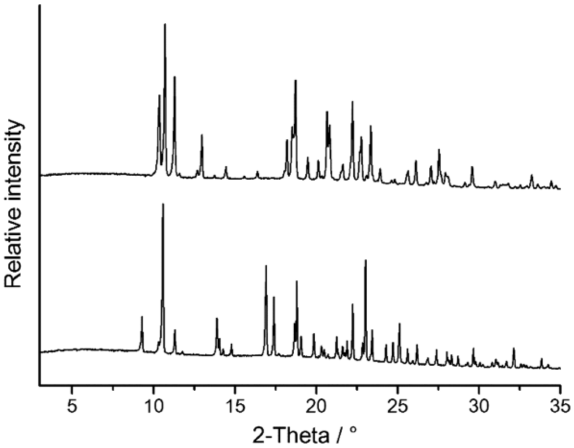

Figure 1. Experimental XRPD pattern of **1-II** (top) and **1-I** (bottom).

During the attempts to synthesize single crystals of **1-II** in acetonitrile a fifth compound with the composition $Ni(NCS)_2$(4-methoxypyridine)$_4$·(MeCN)$_{1.33}$ (**1-MeCN**) was accidently obtained. Unfortunately, for **1-II** no single crystals could be obtained and thus, another way was used for structure determination.

In previous investigations using other transition metal thiocyanates we found that the substitution of Ni^{II} with Co^{II} or Fe^{II} usually leads to the formation of isotypic compounds. In some other cases, the change of the transition metal cations leads to the formation of different structures. Therefore, we tried to prepare a compound with the composition $Fe(NCS)_2$(4-methoxypyridine)$_4$, which might be isotypic to **1-II**. Even if this compound cannot be prepared as a pure phase, XRPD investigations indicate that this crystalline phase (**1-II-Fe**) is isotypic to **1-II**. Single crystals could be easily obtained and were characterized by single-crystal X-ray diffraction. Finally, a Pawley fit of a powder of **1-II** was made using the crystallographic parameters of **1-II-Fe** as the initial values, which shows that both compounds are isotypic (Figure S1, Supporting Information). For all Ni compounds XRPD patterns were calculated and compared with the experimental patterns, which prove that always pure crystalline phases were obtained (Figures S2–S6, Supporting Information). For the calculation of the powder pattern of **1-II**, the lattice parameters determined by the Pawley fit were used.

Thermodynamic Stability of Form 1-I and 1-II

To investigate, which of the two polymorphic modifications represents the thermodynamically stable form at room temperature, a physical mixture of **1-I** and **1-II** in equimolar quantities was prepared, dissolved in water, ethanol, and methanol with an excess of solid forming a suspension, which was stirred for 1 h. As the precipitates were investigated afterwards by XRPD all crystals of **1-II** disappeared and only reflections indicating the presence of **1-I** were observed, which proves that the latter form represents the thermodynamically stable modification at room temperature (Figure 2).

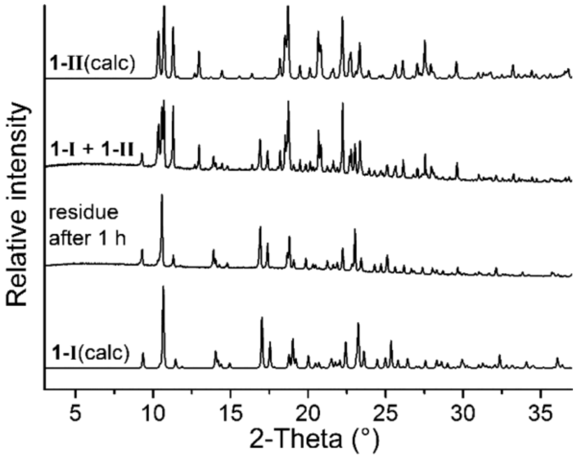

Figure 2. XRPD patterns of an equimolar mixture of compounds **1-I** and **1-II**, the calculated patterns for compounds **1-I** and **1-II** as well as the XRPD pattern of the solid obtained after stirring the mixture of **1-I** and **1-II** for 1 h in methanol as a representative for the experiments obtained from water, ethanol, and methanol.

Additionally measurements using differential scanning calorimetry (DSC) show decomposition at about 214 °C, with very similar decomposition temperatures for **1-I** and **1-II** (Figure S7, Supporting Information). Because this temperature depends on the kinetics of these reactions, no conclusion on the stability of the forms at higher temperatures can be drawn. There is also no sign for a polymorphic transformation of one form into the other below the decomposition temperatures. However, in the case where both forms are related by monotropism an exothermic phase transition is expected, which is usually difficult to detect in DSC measurements. Therefore, these measurements were repeated and stopped before decomposition takes place. If the XRPD patterns of these residues are compared with those calculated for **1-I** and **1-II** no changes are detected (Figures S8 and S9, Supporting Information).

Finally, the unit cell volume of **1-I** and **1-II** was determined by Pawley fits, from which the density was calculated, which shows that the density of **1-II** is higher than that of **1-I** (Table 1). If the density rule is valid, this would mean that **1-II** becomes thermodynamically stable at low temperatures, which indicates that both forms are related by enantiotropism.[62–64]

Table 1. Selected crystal data for **1-I** and **1-II** determined by Pawley fits using powder patterns measured at room temperature.

	1-I	**1-II**
Crystal system	orthorhombic	orthorhombic
Space group	*Pccn*	*Pbca*
a /Å	19.0128(4)	10.2874(3)
b /Å	9.2982(2)	17.0150(4)
c /Å	17.1355(3)	34.2684(7)
α /°	90	90
β /°	90	90
γ /°	90	90
V /Å^3	3029.3(1)	5998.3(2)
Density calcd. /g·cm^{-3}	1.340	1.354

Crystal Structures

The room-temperature stable form **1-I** crystallizes in the orthorhombic space group *Pccn* with the asymmetric unit containing one thiocyanate anion and two 4-methoxypyridine molecules in general positions as well as one Ni^{II} cation being situated on a twofold rotational axis. The Ni cation is octahedrally coordinated by two thiocyanate anions and four 4-methoxypyridine ligands forming discrete complexes (Figure 3).

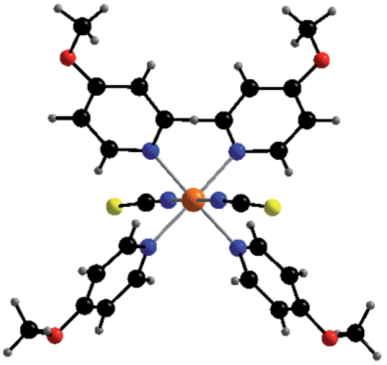

Figure 3. View of the coordination sphere of the Ni^{II} cation in compound **1-I** as a representative for the discrete complexes found in compounds **1-I**, **1-II-Fe**, and **1-MeCN** (Ni: orange; S: yellow; N: blue; C: black; O: red; H: grey). ORTEP plots of **1-I**, **1-II-Fe**, and **1-MeCN** can be found in Figures S10–S12 (Supporting Information).

The Ni–N$_{Py}$ distances amount to 2.111(2) Å and 2.118(2) Å, whereas the corresponding values for the thiocyanate anions are slightly shorter with Ni–N$_{NCS}$ distances amounting to 2.072(2) Å (Table S1, Supporting Information). The N–Ni–N angles deviate slightly from the ideal values indicating a slight distortion of the coordination octahedron. This can be quantified using the octahedral angle variance $\sigma_{\theta\langle oct\rangle}{}^2$ and the mean quadratic elongation λ_{oct} introduced by *Robinson* et al.[65] The resulting values of $\sigma_{\theta\langle oct\rangle}{}^2 = 1.3$ and $\lambda_{oct} = 1.001$ confirm the presence of a minor distortion of the coordination octahedron.

Compound **1-II-Fe** is isotypic to **1-II** and therefore, its structure is discussed as a representative for the form that is thermodynamically metastable at room temperature. **1-II-Fe** crystallizes in the orthorhombic space group *Pbca*. The asymmetric unit consists of two thiocyanate anions, four 4-methoxypyridine molecules, and one Fe^{II} cation, which are all located in general positions. The Fe^{II} cation is octahedrally coordinated by the two anionic as well as the four neutral co-ligands forming discrete complexes (Figure 3). The Fe–N$_{Py}$ and Fe–N$_{NCS}$ distances are slightly larger than those found in **1-I** ranging from 2.198(2) to 2.241(2) Å and 2.115(2) to 2.125(2) Å, which originates from the larger radius of the Fe^{II} cation (Table S2, Supporting Information). The values for the octahedral angle variance ($\sigma_{\theta\langle oct\rangle}{}^2 = 2.9$) and the mean quadratic elongation ($\lambda_{oct} = 1.002$) also indicate a slight distortion of the coordination octahedron. It shall be noted that the coordination octahedron of **1-II-Fe** is stronger distorted than that in **1-I**. To emphasize the differences between the discrete complexes in both modifications **1-I** and **1-II-Fe** an overlay plot is presented in Figure 4, which shows that the orientation and conformation of the ligands is different.

Figure 4. Overlay plot of the discrete complexes found in compound **1-I** (transparent) and **1-II-Fe** (opaque) with labeling of the ligands (Ni/Fe: orange; S: yellow; N: blue; C: black; O: red; H: grey).

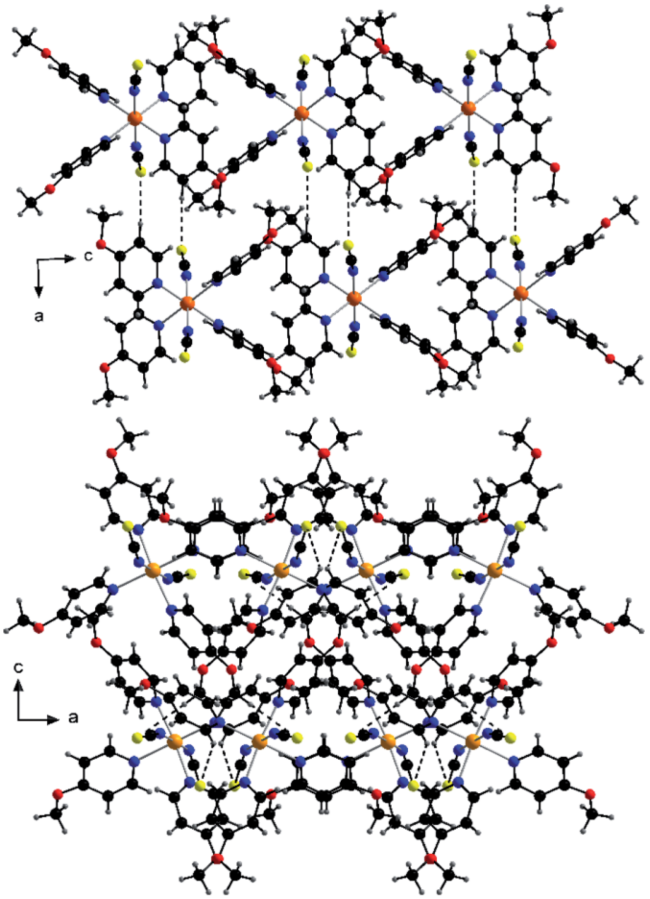

Figure 5. Crystal structure of **1-I** (top) and **1-II-Fe** (bottom) with view along the *b* axis and C–H···S short contacts shown as dashed lines (Ni: orange; S: yellow; N: blue; C: black; O: red; H: grey).

Table 2. Hydrogen bonding /Å,° for **1-I**, **1-II-Fe**, **1-MeCN**, **2**, and **3**.

D–H···*A*	*d*(H···*A*)	*d*(*D*···*A*)	<(*D*H···*A*)
1-I			
C(22)–H(22)..S(1)A	2.92	3.788(2)	152.9
1-II-Fe			
C(16)-H(16B)···S(1)B	2.90	3.839(3)	161.5
C(36)-H(36B)···S(1)C	2.80	3.720(3)	156.7
1-MeCN			
C(22)–H(22)···S(1)	2.99	3.863(4)	157.4
2			
C(16)–H(16B)···S(1)D	2.83	3.788(4)	164.7
C(22)–H(22A)···S(1)E	3.02	3.945(5)	157.7
C(22)–H(22C)···N(1)F	2.56	3.535(5)	171.9
3			
C(16)–H(16B)···O(11)G	2.63	3.522(6)	151.5
C(26)–H(26B)···O(21)H	2.64	3.501(6)	146.1
C(26)–H(26C)···S(1)I	2.83	3.715(5)	151.0

Symmetry codes: A: –*x* + 1, *y* + 1/2, –*z* + 3/2, B: x–1/2, y, –*z* + 3/2, C: *x* + 1/2, –*y* + 3/2, –*z* + 1, D: –*x* + 5/4, *y* + 5/4, *z* + 1/4, E: –*x* + 3/2, –*y* + 1, *z* + 1/2, F: x, *y* + 1/2, *z* + 1/2, G: –*x* + 1, –*y*, –*z* + 2, H: –x, –*y* + 2, –z–1, I: x, *y*, *z*–1.

Two of the four neutral ligands (1 and 4) show a similar orientation of the 4-methoxypyridine ligands in both modifications, whereas this is different for the co-ligands 2 and 3. Large differences are also found in the conformation of the methoxy group in ligand 2, which, in contrast to the methyl groups of the other co-ligands, is rotated by 167.7(4)° along the C_{Py}–O axis in **1-II-Fe**.

Differences are also found in the packing of the discrete complexes in both modifications. In both forms short contacts between H and S atoms of adjacent complexes indicate the presence of weak C–H···S interactions, by which the discrete complexes in **1-I** are connected into layers parallel to the *ab* plane, whereas in **1-II-Fe** they form a three-dimensional network (Figure 5 and Table 2). In **1-II-Fe** some of the six-membered rings of 4-methoxypyridine molecules of neighboring complexes are nearly coplanar with a dihedral angle between the pyridine planes of 4.23(8)°, which is indicative for π–π interactions (Figure 5). However, the intermolecular distance between these molecules amounts to 6.671(1) Å and thus, is too long for such interaction.

Compound **1-MeCN** crystallizes in the cubic space group $P\bar{4}3n$ with the asymmetric unit containing one 4-methoxypyridine ligand in a general position, one thiocyanate anion on a twofold rotational axis, one Ni^{II} cation situated on the intersection point of three twofold rotational axes as well as of one acetonitrile molecule that is located on a threefold rotational axis. The metal cation is octahedrally coordinated by two thiocyanate anions and four 4-methoxypyridine molecules forming discrete complexes analogous to those in **1-I** and **1-II-Fe** (Figure S12, Supporting Information). The Ni–N_{Py} and Ni–N_{NCS} distances amount to 2.120(2) and 2.060(5) Å and are comparable to those in **1-I** (Table S3, Supporting Information). Because of the high symmetry the coordination octahedron is nearly ideal with the octahedral angle variance and the mean quadratic elongation values amounting to $\sigma_{\theta\langle oct\rangle}^2 = 0.2$ and $\lambda_{oct} = 1.000$.

In the crystal structure the discrete complexes are linked by weak C–H···S interactions and are arranged in a way that cavities are formed in which acetonitrile solvate molecules are located (Figure S13, Supporting Information, and Table 2).

The second compound containing acetonitrile also forms discrete complexes. Compound **2** crystallizes in the orthorhombic non-centrosymmetric space group *Fdd*2. The asymmetric unit consists of one thiocyanate anion, one 4-methoxypyridine molecule and one acetonitrile molecule in general positions as well as one Ni^{II} cation that is situated on a twofold rotational axis. The metal cations are octahedrally coordinated by two thiocyanate anions, two 4-methoxypyridine co-ligands, and two acetonitrile molecules (Figure 6 and Figure S14, Supporting Information) with a Ni–N$_{Py}$ distance of 2.105(2) Å and a Ni–N$_{NCS}$ distance of 2.047(3) Å. The distance to the acetonitrile molecules of 2.108(3) Å is comparable to that to the 4-methoxypyridine co-ligand (Table S4, Supporting Information). The coordination polyhedron is slightly distorted with octahedral angle variance and mean quadratic elongation values of $\sigma_{\theta\langle oct\rangle}{}^2 = 3.1$ and $\lambda_{oct} = 1.001$.

Figure 6. View of the coordination sphere of the Ni^{II} cation in compound **2** (Ni: orange; S: yellow; N: blue; C: black; O: red; H: grey). An ORTEP plot of **2** can be found in Figure S14 (Supporting Information).

In the crystal structure of **2** the discrete complexes are arranged into stacks along the crystallographic *b* axis and are connected by weak C–H···S and C–H···N interactions (Figure S15, Supporting Information, and Table 2).

Compound **3** crystallizes in the triclinic space group $P\bar{1}$ with the asymmetric unit consisting of two 4-methoxypyridine molecules and two thiocyanate anions in general positions and two crystallographically independent Ni^{II} cations that are located on centers of inversion (Figure S16, Supporting Information). The metal cations are octahedrally coordinated by four thiocyanate anions, of which two bind via the nitrogen atom and two via the sulfur atom as well as two 4-methoxypyridine molecules in axial positions. The Ni cations are linked into chains by pairs of μ-1,3-bridging anionic ligands (Figure 7 top).

The Ni–N$_{Py}$ distances range from 2.090(4) to 2.121(3) Å and the Ni–N$_{NCS}$ distances from 2.011(4) to 2.045(4) Å, and are comparable to the values known from literature (Table S5, Supporting Information). The Ni–S distances range from 2.525(1) to 2.531(1) Å and are also consistent with the corresponding values reported in the literature. The Ni coordination is slightly distorted with values for the octahedral angle variance and the mean quadratic elongation of $\sigma_{\theta\langle oct\rangle}{}^2 = 6.9$ and $\lambda_{oct} = 1.021$ for Ni1 and $\sigma_{\theta\langle oct\rangle}{}^2 = 5.9$ and $\lambda_{oct} = 1.021$ for Ni2. Along the chains neighboring 4-methoxypyridine co-ligands are nearly perpendicular with dihedral angles between the pyridine ring planes of 84.2(2)° and the Ni–N$_{Py}$ vectors of neighboring cations being tilted by 7.1(2)°. The chains are arranged in a way that the Ni(NCS)$_2$Ni planes of neighboring chains are parallel, which corresponds to one of the typical arrangement in such 1D compounds.[66] The chains are linked by relatively weak intermolecular C–H···S and C–H···O hydrogen bonding into a three-dimensional network (Figure 7 bottom, Table 2).

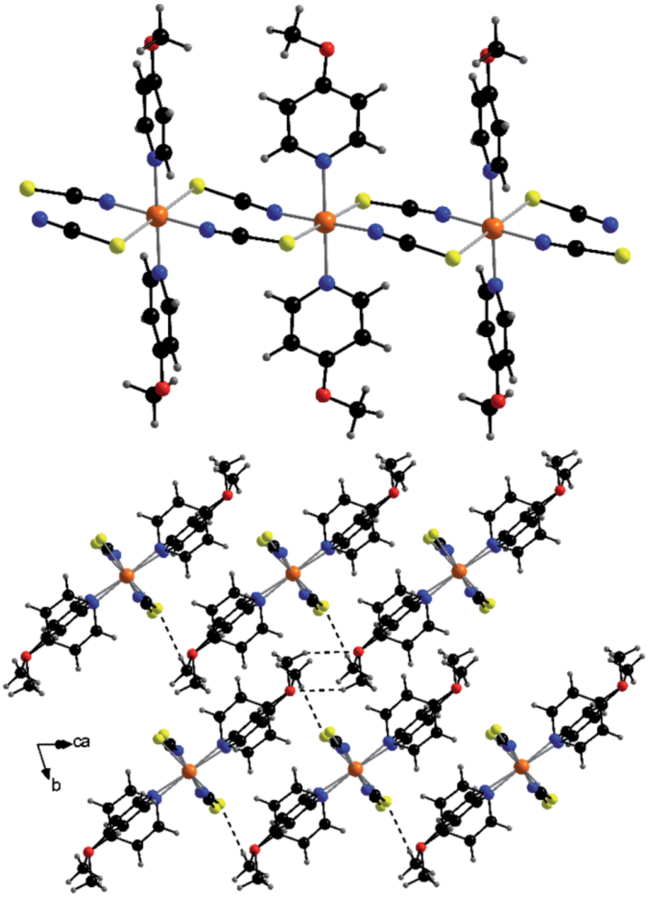

Figure 7. View of a chain in compound **3** (top) and crystal structure with view along the chains (bottom) with C–H···O and C–H···S short contacts shown as dashed lines (Ni: orange; S: yellow; N: blue; C: black; O: red; H: grey). An ORTEP plot of **3** can be found in Figure S16 (Supporting Information).

IR Spectroscopy

To determine the position of the asymmetric CN stretching band of the thiocyanate anions IR spectroscopic measurements were performed (Figures S17–21, Supporting Information, Table 3). For compounds containing N-terminally coordinated

Table 3. Wavenumbers of the asymmetric CN stretching vibration of the thiocyanate anions in compounds **1-I**, **1-II**, **1-MeCN**, **2**, and **3** in cm^{-1}.

	1-I	**1-II**	**1-MeCN**	**2**	**3**
Position	2071	2070	2082	2083	2113, 2126

thiocyanate anions the CN stretching vibration is usually found below 2100 cm^{-1}, whereas for those containing μ-1,3 bridging thiocyanate anions this vibration is observed above 2100 cm^{-1}.[67]

The IR spectrum of compound **1-I** shows a band at 2071 cm^{-1}, which is in good agreement with what is expected for N-terminally coordinated thiocyanate anions. For the polymorphic modification **1-II** the corresponding band is found at 2070 cm^{-1}, which is expected because of the structural similarity of both discrete complexes. In fact, two different values are expected because this form contains two crystallographically independent anions but obviously, they cannot be resolved. In the IR spectrum of compound **1-MeCN** the CN stretching vibration is shifted to 2082 cm^{-1}, indicating that the incorporated acetonitrile solvate molecules might have an influence on this vibration. The two signals at 2285 cm^{-1} and 2313 cm^{-1} can be assigned to the CN stretch of the acetonitrile solvent molecules. For compound **2** the value of the CN stretching vibration (2083 cm^{-1}) is very similar to that in **1-MeCN** but still in the range expected for N-terminally bonded thiocyanate anions. In contrast, for compound **3** that contains μ-1,3-bridging thiocyanate anions the CN stretching vibration is shifted above 2100 cm^{-1}. Two different values at 2113 cm^{-1} and 2126 cm^{-1} are observed that originate from the two crystallographically independent thiocyanate anions. In contrast to **1-II** these two values can be resolved, which might be traced back to the fact, that each of the thiocyanate N atoms is connected to a crystallographically different metal cation.

Thermoanalytical Investigations

As shown in this work most of the compounds obtained from solution are discrete complexes containing only terminally bonded thiocyanate anions. In this context the question arose if these compounds can be transformed by thermal degradation into the chain compound **3** or into a different polymorphic or isomeric modification as shown in recent work.[45] It is also of interest, which of the two polymorphic modifications **1-I** or **1-II** is obtained by removal of the acetonitrile solvate molecules in compound **1-MeCN**. Therefore, compounds **1-MeCN**, **1-I**, **1-II**, and **2** were investigated by simultaneous thermogravimetry and differential scanning calorimetry (TG-DSC). For clarity only the thermogravimetric curves are shown in Figure 8 but complete TG, DSC, and DTG curves can be found in Figures S22–S25 (Supporting Information).

Upon heating **1-MeCN** decomposes in three different steps with each step accompanied by endothermic events in the DSC curve (Figure 8 and Figure S22, Supporting Information). The first mass loss is slightly higher than that calculated for the removal of 1.33 acetonitrile molecules per formula unit (Δm_{calcd} = 8.2 %) indicating the presence of additional solvent molecules in this compound. This is expected as single crystal structure analysis showed that **1-MeCN** contains a small amount of disordered solvent molecules. However, upon further heating two mass steps are observed, which are in reasonable agreement with the removal of two 4-methoxypyridine ligands per formula unit (Δm_{calcd} = 32.8 %) each.

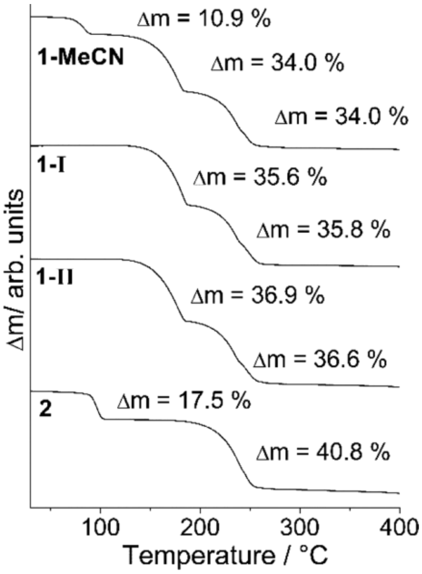

Figure 8. TG curves of **1-MeCN**, **1-I**, **1-II**, and **2** at 4 K·min^{-1} in a nitrogen atmosphere.

Compounds **1-I**, **1-II**, and **2** decompose in two steps upon heating and for each of these steps an endothermic event is observed in the DSC curve (Figures S23–S25, Supporting Information). For **1-I** and **1-II** the mass loss in each step is very similar for both compounds and in good agreement with that expected for the removal of two 4-methoxypyridine molecules in each step (Δm_{calcd} = 35.7 %). For the acetonitrile compound **2** the mass loss of the first mass step corresponds to that calculated for the removal of the MeCN molecules (Δm_{calcd} = 17.3 %), whereas in the last step the 4-methoxypyridine ligands are removed.

To identify the intermediates that formed after the first TG step of compound **1-MeCN** a TG measurement was stopped after the first step and the residue was investigated using XRPD, which shows that polymorph **1-I** formed (Figure 9).

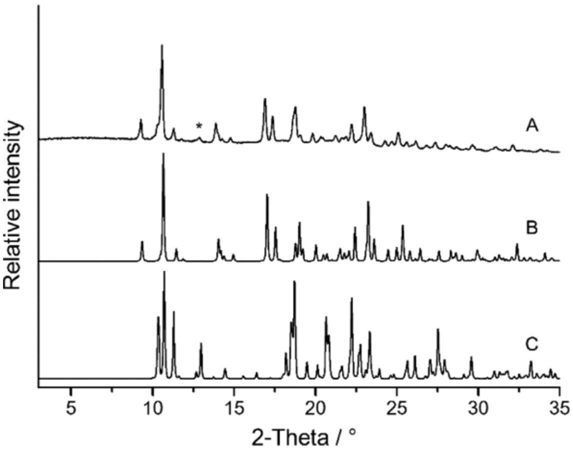

Figure 9. XRPD pattern of the residue obtained after the first step of the thermal degradation of compound **1-MeCN** (A), and the calculated patterns for **1-I** (B) and **1-II** (C). The reflection marked with an asterisk does not correspond to the XRPD pattern of **1-I**.

There is an additional reflection, which indicates that a further and unknown crystalline compound was also obtained.

Similar experiments for **1-I**, **1-II**, and **2** prove that they transform into the chain compound **3** after removal of half of the 4-methoxypyridine ligands for compounds **1-I** and **1-II** and after complete removal of the acetonitrile molecules in compound **2** (Figure 10). There is no indication for the formation of an additional crystalline phase.

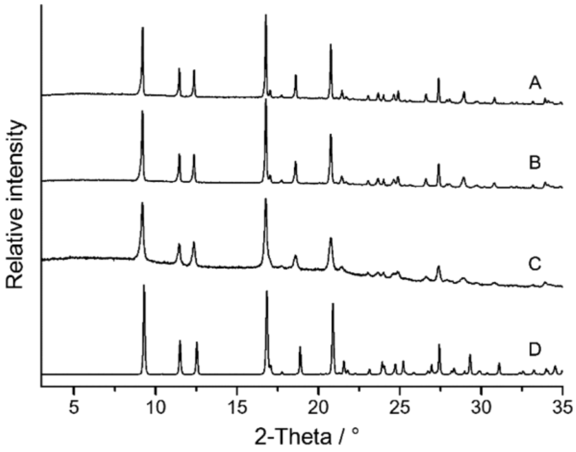

Figure 10. XRPD pattern of the residues obtained after the first step of the thermal degradation of compound **1-I** (A), **1-II** (B), and **2** (C) as well as the calculated pattern for **3** (D).

Subsequent investigations using time-resolved XRPD showed that compound **2** loses the acetonitrile molecules already at room-temperature and transforms into compound **3** within a few hours (Figure 11). However, under acetonitrile atmosphere it is stable over a long period. To investigate the reversibility of the acetonitrile removal, compound **3** was kept in a MeCN atmosphere for 14 d, but no changes were observed (Figure S26, Supporting Information).

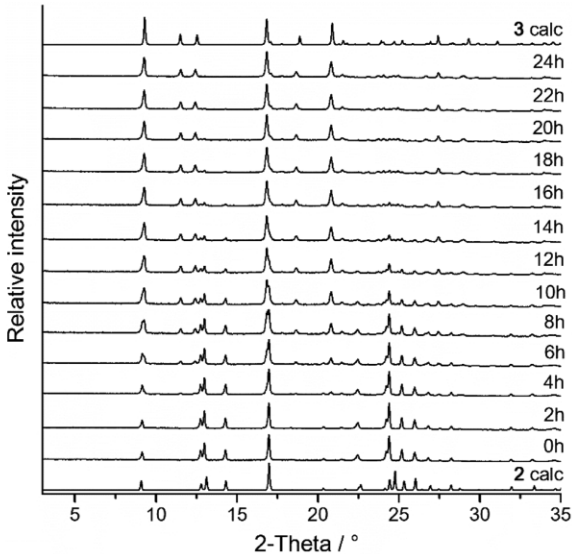

Figure 11. Time dependent XRPD pattern of **2** measured each 2 h at room temperature.

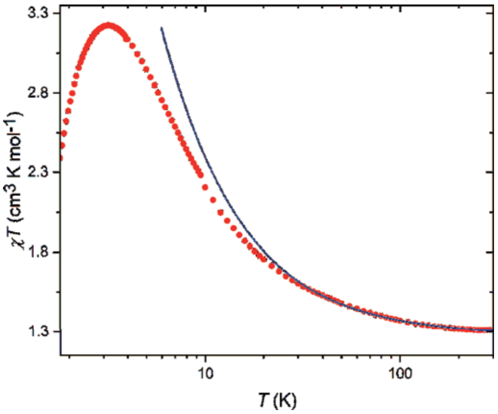

Figure 12. Temperature dependence of the magnetic susceptibility χ measured at 1 kOe for compound **3** presented as the χT product.

Magnetic Properties

The magnetic properties were studied only for compound **3**, because for the remaining presented structures only single-ion magnetic properties are expected, due to lack of exchange paths between the magnetic Ni ions. For **3**, the temperature dependence of the magnetic susceptibility χ is presented in Figure 12. Starting from room temperature, the χT product increases as the temperature decreases, which means that the exchange interaction J along the $Ni(NCS)_2$ chains is ferromagnetic. To quantify J, the Heisenberg chain Hamiltonian with isotropic spins ($S = 1$) was used:

$$\hat{H} = -J\sum_n \vec{S}_n \vec{S}_{n+1} + g\mu_B H_z \sum_n S_n^z$$

The values J and g were determined by fitting the experimental data above 30 K using the approximation formula valid for ferromagnetic exchange $J > 0$:[45]

$$\chi T = \frac{N_A \mu_B^2}{k_B} g^2 \left(\frac{a_0 + a_1 x + a_2 x^2}{1 + b_1 x + b_2 x^2 + b_3 x^3}\right)^c$$

$$\begin{aligned} &x = J/T, && c = -0.81086, \\ &a_0 = 1.65273, && a_1 = 2.05175, && a_2 = 2.84018, \\ &b_1 = 2.88478, && b_2 = 4.65762, && b_3 = 4.30349. \end{aligned}$$

The values obtained are $J = 5.92(10)$ K and $g = 2.21(1)$.[45] This J value is at the lower limit of those reported for linear $Ni(NCS)_2$ chains but it is still higher than values recently found for corrugated chains and therefore is in agreement with previous investigations.[45,61]

Below 30 K the course of $\chi T(T)$ experimental points differs from the extrapolated curve, which is probably due to an anisotropy of the single Ni^{II} ion and interchain interactions, which are not accounted for in the above Hamiltonian. The low-temperature dependence of the susceptibility measured at 100 Oe is shown in Figure 13 top. There is no difference between zero-field cooled and field cooled susceptibility (Figure S27, Supporting Information) and the out-of-phase ac susceptibility is practically zero (Figure S28, Supporting Information). All these low field susceptibility data show a $\chi(T)$ maximum around 2.05 K, which suggests an onset of magnetic ordering due to antiferromagnetic interchain interactions. To check if the ordering transition really occurs, specific heat measurements were performed (Figure S29, Supporting Information).

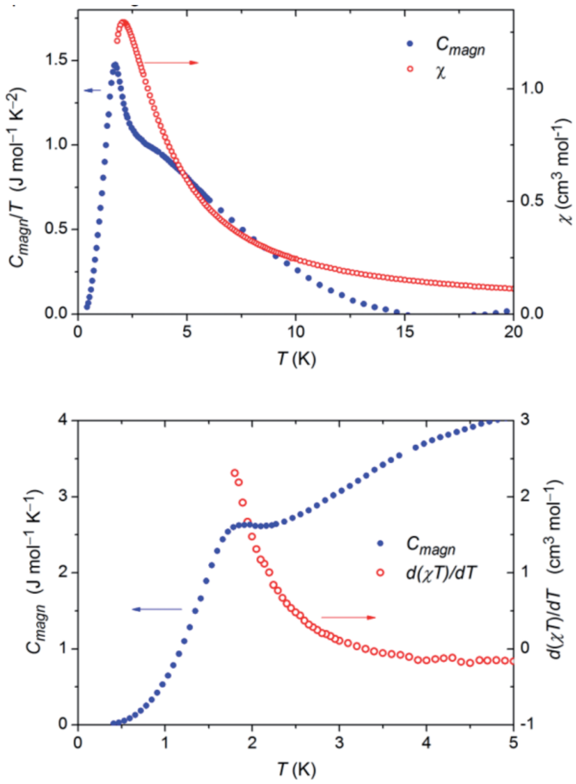

Figure 13. Temperature dependence of the susceptibility χ measured at 100 Oe and the magnetic contribution to the specific heat over temperature C_{magn}/T (top) as well as C_{magn} together with the $d(\chi T)/dT$ derivative (bottom) for compound **3**.

Above 10 K the dominant contribution to the specific heat originates from the crystal lattice. This lattice contribution to the specific heat was estimated by fitting the Debye phonon model in the range from 16 to 20 K and extrapolating to lower temperatures. The magnetic contribution to the specific heat C_{magn} that was obtained by subtracting the lattice contribution is also shown in Figure 13 top. The small peak of C_{magn} that is visible at $T_c = 1.91(5)$ K corresponds to the magnetic ordering. There is also a broad peak at around 6 K, which originates from the exchange interaction along the $Ni(NCS)_2$ chains and zero-field splitting of Ni^{II}. The determined magnetic entropy change from 0.4 to 16 K equals $\Delta S = 7.4$ J·mol^{-1}·K^{-1}, which is slightly lower than the theoretical value $R \cdot \ln(2S + 1) = 9.13$ J·mol^{-1}·K^{-1}.

The positions of C_{magn} and χ maxima are not exactly at the same temperature (see Figure 13 top). The reason may be that for an antiferromagnetic ordering, the critical temperature T_c should be determined from magnetic data as the position of the $d(\chi T)/dT$ maximum, which in some cases is shifted from the position of the $\chi(T)$ maximum.[68,69] To check this, $d(\chi T)/dT$ was plotted together with C_{magn} for comparison as a function of temperature (Figure 13 bottom). However using these data the $d(\chi T)/dT$ maximum is not observed due to the experimentally available temperature range, which is limited to 1.8 K.

Conclusions

The reaction of $Ni(NCS)_2$ and 4-methoxypyridine leads to the formation of several compounds with 4-methoxypyridine as co-ligand, with most of them consisting of discrete complexes, in which the Ni^{II} cations are octahedrally coordinated by four co-ligands and two terminally N-bonded anions. This also includes two polymorphic modifications, for which the thermodynamic stability at room-temperature was investigated. The structure of the thermodynamically metastable form was clarified by crystallization of the corresponding Fe compound, which shows that crystallization of compounds with cations of similar coordination behavior is an alternative tool to extract structural information in those cases, in which no single crystals are available. Both discrete complexes with the composition $Ni(NCS)_2$(4-methoxypyridine)$_4$ lose half of their 4-methoxypyridine ligands upon heating transforming into a coordination polymer with the composition [$Ni(NCS)_2$(4-methoxypyridine)$_2$]$_n$, in which the cations are linked by pairs of anionic ligands into linear chains. This transformation also occurs for $Ni(NCS)_2$(4-methoxypyridine)$_2$(MeCN)$_2$, but in this case the acetonitrile molecules are emitted. For [$Ni(NCS)_2$(4-methoxypyridine)$_2$]$_n$ the exchange constant was determined by magnetic measurements leading to a value of $J = 5.92(10)$ K, which is at the lower limit compared to the corresponding values found for similar compounds with linear chains, but still higher than what is usually found for corrugated chains. Heat capacity measurement proved that antiferromagnetic ordering occurs at 1.91(5) K.

Experimental Section

Synthesis: $NiSO_4 \cdot 6H_2O$ was obtained from Merck, $Ba(NCS)_2 \cdot 3H_2O$ was obtained from Alfa Aesar and 4-methoxypyridine from TCI. All chemicals were used without further purification. If not noted otherwise all crystalline powders were prepared by stirring the reactants in solution at room temperature. The residues were filtered off and dried in air.

$Ni(NCS)_2$: $Ni(NCS)_2$ was prepared by the reaction of equimolar amounts of $NiSO_4 \cdot 6H_2O$ and $Ba(NCS)_2 \cdot 3H_2O$ in water. The resulting white precipitate of $BaSO_4$ was filtered off and the filtrate was concentrated to complete dryness resulting in a greenish-brown residue of $Ni(NCS)_2$.

Synthesis of 1-I: To a solution of $Ni(NCS)_2$ (87.4 mg, 0.50 mmol) in 4.0 mL water 4-methoxypyridine (203.0 µL, 2.00 mmol) was added. After stirring the mixture for 4 d, the blue residue was filtered of and washed with water. Single crystals were obtained by layering a solution of $Ni(NCS)_2$ (26.2 mg, 0.15 mmol) in 2.0 mL water with 2.0 mL of ethyl ether. 4-Methoxypyridine (60.8 mL, 0.60 mmol) was carefully added to the mixture and after 1 d deep blue crystals were obtained. $C_{26}H_{28}N_6NiO_4S_2$ (611.3681 g·mol^{-1}): calcd. C 51.08, H 4.62, N 13.75, S 10.49 %; found: C 51.04, H 4.66, N 13.70, S 10.58 %.

Synthesis of 1-II: To a solution of $Ni(NCS)_2$ (87.4 mg, 0.50 mmol) in 1.0 mL water 4-methoxypyridine (76.2 µL, 0.75 mmol) was added.

The resulting blue precipitate was filtered of immediately and dried in air. $C_{26}H_{28}N_6NiO_4S_2$ (611.3681 g·mol^{-1}): calcd. C 51.08, H 4.62, N 13.75, S 10.49 %; found: C 51.04, H 4.78, N 13.59, S 10.58 %.

Synthesis of 1-II-Fe: Single crystals were prepared in a similar way to those obtained for compound **1-I**. A mixture of $FeSO_4·7H_2O$ (27.8 mg, 0.10 mmol) and KSCN (19.5 mg, 0.20 mmol) in 1.0 mL water was layered with 2.0 mL ethyl ether. Subsequently 4-methoxypyridine (60.8 µL, 0.60 mmol) was carefully added to the mixture. After one day light yellow crystals were obtained, which were suitable for X-ray structure determination.

Synthesis of 1-MeCN: $Ni(NCS)_2$ (43.7 mg, 0.25 mmol) was stirred with 4-methoxypyridine (101.6 µL, 1.00 mmol) in 2.5 mL MeCN in a closed culture tube at 90 °C until complete dissolution of the reactants was observed. The solution was let to cool to room temperature, upon which blue crystals suitable for single crystal diffraction formed. For powders of this compound the crystals obtained were grinded and the resulting powder stored in an acetonitrile atmosphere. $C_{28.67}H_{32}N_{7.33}NiO_4S_2$ (666.1048 g·mol^{-1}): calcd. C 51.69, H 4.84, N 15.42, S 9.63 %; found: C 51.97, H 4.79, N 15.80, S 9.34 %.

Synthesis of 2: A mixture of $Ni(NCS)_2$ (43.7 mg, 0.25 mmol) and 4-methoxypyridine (25.4 µL, 0.25 mmol) was stirred in 3.0 mL acetonitrile until complete dissolution occurred. The resulting solution was concentrated at ambient conditions until a blue precipitate was observed, which was filtered of and stored under acetonitrile atmosphere. Single crystals were grown from the filtrate by slow evaporation of the solvent. It shall be noted that compound **2** was only obtained as a phase pure powder after a complete dissolution of the reactants and subsequent removal of the solvent. If the product was isolated before a clear solution had formed and compound **3** was obtained. $C_{18}H_{20}N_6NiO_2S_2$ (475.2178 g·mol^{-1}): calcd. C 45.49, H 4.24, N 17.68, S 13.50 %; found: C 42.26, H 3.93, N 16.49, S 13.54 %. The large differences in the elemental analysis can be traced back to the fact that this compound was already decomposed at room temperature.

Synthesis of 3: A microcrystalline powder on larger scale was synthesized by stirring a mixture of $Ni(NCS)_2$ (174.8 mg, 1.00 mmol) and 4-methoxypyridine (101.5 µL, 1.00 mmol) in 3.0 mL of ethanol for 3 d. Single crystals were obtained by layering a solution of $Ni(NCS)_2$ (52.4 mg, 0.30 mmol) in 2.0 mL water with 2.0 mL ethyl ether and carefully adding 4-methoxypyridine (15.2 µL, 0.15 mmol). After several days green crystals suitable for X-ray structure determination formed. $C_{14}H_{14}N_4NiO_2S_2$ (393.1128 g·mol^{-1}): calcd. C 42.78, H 3.59 N 14.25, S 16.31 %; found: C 42.34, H 3.65, N 14.14, S 16.88 %.

Single-crystal Structure Analysis: Data collection was performed with an imaging plate diffraction system (IPDS-2) from STOE & CIE using Mo-K_α radiation. Structure solution was performed with SHELXS-97[70] or SHELXT[71] and structure refinements were performed against F^2 using SHELXL-2014.[72] A numerical absorption correction was applied using programs X-RED and X-SHAPE of the program package X-Area.[73] All non-hydrogen atoms were refined with anisotropic displacement parameters. The C–H hydrogen atoms were positioned with idealized geometry (methyl H atoms were allowed to rotate but not to tip) and were refined isotropically with $U_{iso}(H) = 1.2\ U_{eq}(C)$ (1.5 for methyl H atoms) using a riding model. The absolute structure of **1-MeCN** and **2** was determined and is in agreement with the selected setting [Flack-x parameter: –0.030(8) for **1-MeCN** and –0.002(9) for **2**]. After the structure refinement of **1-MeCN** a very small amount of residual electron density was found in the cavities indicating the presence of disordered solvent. Therefore the data were corrected for disordered solvent using the SQUEEZE routine in PLATON. For this structure PLATON detected pseudo-symmetry leading to the centrosymmetric space group $Pn\bar{3}n$. Refinement in this space group yielded significantly worse R values and symmetry related disorder of the methoxy groups. Because this was not the case in the non-centrosymmetric space group $P\bar{4}3n$, where the absolute structure can also be determined, this space group was chosen. The crystal of compound **2** was merohedrally twinned and therefore, a twin refinement was performed leading to a BASF parameter of 0.42 (2).

Table 4. Selected crystal data and details of the structure refinements.

	1-MeCN	**1-I**	**1-II-Fe**	**2**	**3**
formula	$C_{28.67}H_{32}N_{7.33}NiO_4S_2$	$C_{26}H_{28}N_6NiO_4S_2$	$C_{26}H_{28}FeN_6O_4S_2$	$C_{18}H_{20}N_6NiO_2S_2$	$C_{14}H_{14}N_4NiO_2S_2$
MW /g·mol^{-1}	666.11	611.37	608.51	475.23	393.12
Crystal system	cubic	orthorhombic	orthorhombic	orthorhombic	triclinic
Space group	$P\bar{4}3n$	$Pccn$	$Pbca$	$Fdd2$	$P\bar{1}$
a /Å	17.2262(5)	18.8975(5)	10.2901(2)	38.9287(3)	8.9076(7)
b /Å	17.2262(5)	9.2301(2)	16.7120(3)	8.0570(7)	10.4170(9)
c /Å	17.2262(5)	16.9150(5)	34.5051(10)	14.3752(5)	10.8294(9)
a /°	90	90	90	90	65.877(6)
β /°	90	90	90	90	67.720(6)
γ /°	90	90	90	90	83.224
V /Å^3	5111.7(4)	2950.41(13)	5933.8(2)	4508.8(6)	847.83(13)
T /K	200(2)	170(2)	170(2)	170(2)	170(2)
Z	6	4	8	8	2
D_{calcd} /g·cm^{-3}	1.298	1.376	1.362	1.400	1.540
μ /mm^{-1}	0.734	0.840	0.690	1.071	1.403
θ_{max} /°	26.991	27.001	25.093	27.003	25.198
Measured refl.	17673	19356	24654	8978	6127
Unique refl.	1846	3215	5269	2476	3008
Refl. $F_o > 4\sigma(F_o)$	1589	2734	4202	2328	2362
Parameter	101	179	356	136	214
R_{int}	0.0283	0.0355	0.1007	0.0289	0.0950
R_1 $[F_0 > 4\sigma F_0)]$	0.0411	0.0358	0.0433	0.0299	0.0591
wR_2 [all data]	0.1154	0.0968	0.01153	0.0812	0.1751
Flack x	–0.030(8)	–	–	–0.002(9)	–
GOF	1.093	1.070	1.101	1.072	1.057
$\Delta\rho_{max/min}$ /e·Å^{-3}	0.180/ –0.344	0.283/ –0.342	0.635/ –0.580	0.303/ –0.288	0.599/ –0.967

Selected crystal data and details of the structure refinements are summarized in Table 4.

Crystallographic data (excluding structure factors) for the structures in this paper have been deposited with the Cambridge Crystallographic Data Centre, CCDC, 12 Union Road, Cambridge CB21EZ, UK. Copies of the data can be obtained free of charge on quoting the depository numbers CCDC-1856759 (**1-I**), CCDC-1856762 (**1-II-Fe**), CCDC-1856761 (**1-MeCN**), CCDC-1856760 (**2**), and CCDC-1856758 (**3**) (Fax: +44-1223-336-033; E-Mail: deposit@ccdc.cam.ac.uk, http://www.ccdc.cam.ac.uk)

X-ray Powder Diffraction (XRPD): The measurements were performed with Cu-$K_{\alpha 1}$ radiation (λ = 1.540598 Å) with a Stoe Transmission Powder Diffraction System (STADI P) that is equipped with a MYTHEN 1 K detector and a Johansson-type Ge(111) monochromator.

Magnetic Measurements: Magnetic measurements were performed with a MPMS-5XL squid magnetometer from Quantum Design. Powder was lightly pressed and soaked in nujol to immobilize sample grains. The diamagnetic contributions of sample holders and the core diamagnetism were subtracted, using measured and calculated values, respectively.

Specific Heat Measurements: Specific heat was measured by the relaxation technique with a Quantum Design PPMS equipped with He-3 cooling. Powders were pressed into pellets with no binder. Apiezon N grease was used to ensure thermal contact of the samples with the microcalorimeter.

IR Spectroscopy: The IR spectra were measured with an ATI Mattson Genesis Series FTIR Spectrometer, control software: WINFIRST, from ATI Mattson.

Elemental Analysis: CHNS analysis was performed with an EURO EA elemental Analyser, fabricated by EURO VECTOR Instruments.

Thermogravimetry and Differential Scanning Calorimetry (TG-DSC): TG-DSC measurements were performed in a dynamic nitrogen atmosphere in Al_2O_3 crucibles using a STA-PT 1600 thermobalance from Linseis. The instrument was calibrated using standard reference materials. All measurements were performed with a flow rate of 75 mL·min^{-1} and were corrected for buoyancy.

Differential Scanning Calorimetry (DSC): The DSC measurements were performed with a DSC 1 Star System with STARe Excellence Software from Mettler-Toledo AG. The instrument was calibrated using standard reference materials.

Supporting Information (see footnote on the first page of this article): XRPD patterns, ORTEP plots, IR spectra, DTA-DTG curves, ZFC/FC and ac magnetic data.

Acknowledgements

This project was supported by the Deutsche Forschungsgemeinschaft (Project No. NA 720/5–2) and the State of Schleswig-Holstein. We thank *Prof. Dr. Wolfgang Bensch* for access to his experimental facilities.

Keywords: 1D coordination compound; Crystal structure; Thermal properties; Polymorphism; Magnetic properties

References

[1] J. Martínez-Lillo, J. Faus, F. Lloret, M. Julve, *Coord. Chem. Rev.* **2015**, *289–290*, 215.
[2] X. Y. Wang, C. Avendano, K. R. Dunbar, *Chem. Soc. Rev.* **2011**, *40*, 3213.
[3] J. S. Miller, *Chem. Soc. Rev.* **2011**, *40*, 3266.
[4] G. A. Craig, M. Murrie, *Chem. Soc. Rev.* **2015**, *44*, 2135.
[5] M. Kurmoo, *Chem. Soc. Rev.* **2009**, *38*, 1353.
[6] M. Murrie, *Chem. Soc. Rev.* **2010**, *39*, 1986.
[7] G. Aromi, D. Aguila, P. Gamez, F. Luis, O. Roubeau, *Chem. Soc. Rev.* **2012**, *41*, 537.
[8] D.-F. Weng, Z.-M. Wang, S. Gao, *Chem. Soc. Rev.* **2011**, *40*, 3157.
[9] J. Mroziński, *Coord. Chem. Rev.* **2005**, *249*, 2534.
[10] S. Tanase, J. Reedijk, *Coord. Chem. Rev.* **2006**, *250*, 2501.
[11] R. Mas-Balleste, J. Gomez-Herrero, F. Zamora, *Chem. Soc. Rev.* **2010**, *39*, 4220.
[12] L. Bogani, C. Sangregorio, R. Sessoli, D. Gatteschi, *Angew. Chem.* **2005**, *117*, 5967.
[13] S. Dhers, H. L. C. Feltham, S. Brooker, *Coord. Chem. Rev.* **2015**, *296*, 24.
[14] R. Lescouëzec, L. M. Toma, J. Vaissermann, M. Verdaguer, F. S. Delgado, C. Ruiz-Pérez, F. Lloret, M. Julve, *Coord. Chem. Rev.* **2005**, *249*, 2691.
[15] H.-L. Sun, Z.-M. Wang, S. Gao, *Coord. Chem. Rev.* **2010**, *254*, 1081.
[16] C. Coulon, V. Pianet, M. Urdampilleta, R. Clérac, in *Molecular Nanomagnets and Related Phenomena* (Ed.: S. Gao), Springer Berlin Heidelberg, Berlin, Heidelberg, **2015**, p. 143.
[17] J. Cernák, M. Orendác, I. Potocnák, J. Chomic, A. Orendácová, J. Skorsepa, A. Feher, *Coord. Chem. Rev.* **2002**, *224*, 51.
[18] M. A. M. Abu-Youssef, F. A. Mautner, R. Vicente, *Inorg. Chem.* **2007**, *46*, 4654.
[19] M. Rams, E. V. Peresypkina, V. S. Mironov, W. Wernsdorfer, K. E. Vostrikova, *Inorg. Chem.* **2014**, *53*, 10291.
[20] M. A. M. Abu-Youssef, V. Langer, D. Luneau, E. Shams, M. A. S. Goher, L. Öhrström, *Eur. J. Inorg. Chem.* **2008**, *2008*, 112.
[21] J.-Y. Zhang, C.-M. Liu, D.-Q. Zhang, S. Gao, D.-B. Zhu, *Inorg. Chem. Commun.* **2007**, *10*, 897.
[22] M. S. Goher, F. Mautner, *Transition Met. Chem.* **1999**, *24*, 454.
[23] H. Miyasaka, M. Julve, M. Yamashita, R. Clérac, *Inorg. Chem.* **2009**, *48*, 3420.
[24] M. Yuan, F. Zhao, W. Zhang, Z.-M. Wang, S. Gao, *Inorg. Chem.* **2007**, *46*, 11235.
[25] J.-F. Guo, X.-T. Wang, B.-W. Wang, G.-C. Xu, S. Gao, L. Szeto, W.-T. Wong, W.-Y. Wong, T.-C. Lau, *Chem. Eur. J.* **2010**, *16*, 3524.
[26] Z.-X. Li, Y.-F. Zeng, H. Ma, X.-H. Bu, *Chem. Commun.* **2010**, *46*, 8540.
[27] J. H. Yoon, J. W. Lee, D. W. Ryu, S. W. Yoon, B. J. Suh, H. C. Kim, C. S. Hong, *Chem. Eur. J.* **2011**, *17*, 3028.
[28] P. S. Mukherjee, S. Dalai, E. Zangrando, F. Lloret, N. R. Chaudhuri, *Chem. Commun.* **2001**, 1444.
[29] J. Boonmak, M. Nakano, S. Youngme, *Dalton Trans.* **2011**, *40*, 1254.
[30] J. L. Guillet, I. Bhowmick, M. P. Shores, C. J. A. Daley, M. Gembicky, J. A. Golen, A. L. Rheingold, L. H. Doerrer, *Inorg. Chem.* **2016**, *55*, 8099.
[31] S. S. Massoud, A. E. Guilbeau, H. T. Luong, R. Vicente, J. H. Albering, R. C. Fischer, F. A. Mautner, *Polyhedron* **2013**, *54*, 26.
[32] M. Monfort, C. Bastos, C. Diaz, J. Ribas, X. Solans, *Inorg. Chim. Acta* **1994**, *218*, 185.
[33] J. Mroziński, J. Kłak, R. Kruszyński, *Polyhedron* **2008**, *27*, 1401.
[34] M. Mousavi, V. Bereau, C. Duhayon, P. Guionneau, J.-P. Sutter, *Chem. Commun.* **2012**, *48*, 10028.
[35] J. Palion-Gazda, B. Machura, F. Lloret, M. Julve, *Cryst. Growth Des.* **2015**, *15*, 2380.
[36] B. Żurowska, J. Mroziński, M. Julve, F. Lloret, A. Maslejova, W. Sawka-Dobrowolska, *Inorg. Chem.* **2002**, *41*, 1771.

[37] C. Näther, S. Wöhlert, J. Boeckmann, M. Wriedt, I. Jess, *Z. Anorg. Allg. Chem.* **2013**, *639*, 2696.

[38] E. Shurdha, S. H. Lapidus, P. W. Stephens, C. E. Moore, A. L. Rheingold, J. S. Miller, *Inorg. Chem.* **2012**, *51*, 9655.

[39] E. Shurdha, C. E. Moore, A. L. Rheingold, S. H. Lapidus, P. W. Stephens, A. M. Arif, J. S. Miller, *Inorg. Chem.* **2013**, *52*, 10583.

[40] M. Kabesová, R. Boca, M. Melník, D. Valigura, M. Dunaj-Jurco, *Coord. Chem. Rev.* **1995**, *140*, 115.

[41] D. A. Buckingham, *Coord. Chem. Rev.* **1994**, *135*, 587.

[42] F. A. Mautner, M. Scherzer, C. Berger, R. C. Fischer, R. Vicente, S. S. Massoud, *Polyhedron* **2015**, *85*, 20.

[43] F. A. Mautner, R. C. Fischer, L. G. Rashmawi, F. R. Louka, S. S. Massoud, *Polyhedron* **2017**, *124*, 237.

[44] S. S. Massoud, M. Dubin, A. E. Guilbeau, M. Spell, R. Vicente, P. Wilfling, R. C. Fischer, F. A. Mautner, *Polyhedron* **2014**, *78*, 135.

[45] T. Neumann, M. Ceglarska, M. Rams, L. S. Germann, R. E. Dinnebier, S. Suckert, I. Jess, C. Näther, *Inorg. Chem.* **2018**, *57*, 3305.

[46] S. Suckert, M. Rams, L. S. Germann, D. M. Cegiełka, R. E. Dinnebier, C. Näther, *Cryst. Growth Des.* **2017**, *17*, 3997.

[47] S. Wöhlert, T. Fic, Z. Tomkowicz, S. G. Ebbinghaus, M. Rams, W. Haase, C. Näther, *Inorg. Chem.* **2013**, *52*, 12947.

[48] S. Wöhlert, M. Wriedt, T. Fic, Z. Tomkowicz, W. Haase, C. Näther, *Inorg. Chem.* **2013**, *52*, 1061.

[49] S. Wöhlert, T. Runčevski, R. E. Dinnebier, S. G. Ebbinghaus, C. Näther, *Cryst. Growth Des.* **2014**, *14*, 1902.

[50] J. Werner, T. Runčevski, R. Dinnebier, S. G. Ebbinghaus, S. Suckert, C. Näther, *Eur. J. Inorg. Chem.* **2015**, *2015*, 3236.

[51] J. Werner, M. Rams, Z. Tomkowicz, T. Runčevski, R. E. Dinnebier, S. Suckert, C. Näther, *Inorg. Chem.* **2015**, *54*, 2893.

[52] S. Wöhlert, J. Boeckmann, I. Jess, C. Näther, *CrystEngComm* **2012**, *14*, 5412.

[53] S. Wöhlert, U. Ruschewitz, C. Näther, *Cryst. Growth Des.* **2012**, *12*, 2715.

[54] M. Rams, M. Böhme, V. Kataev, Y. Krupskaya, B. Büchner, W. Plass, T. Neumann, Z. Tomkowicz, C. Näther, *Phys. Chem. Chem. Phys.* **2017**, *19*, 24534.

[55] M. Rams, Z. Tomkowicz, M. Böhme, W. Plass, S. Suckert, J. Werner, I. Jess, C. Näther, *Phys. Chem. Chem. Phys.* **2017**, *19*, 3232.

[56] S. Suckert, M. Rams, M. Böhme, L. S. Germann, R. E. Dinnebier, W. Plass, J. Werner, C. Näther, *Dalton Trans.* **2016**, *45*, 18190.

[57] J. Werner, Z. Tomkowicz, T. Reinert, C. Näther, *Eur. J. Inorg. Chem.* **2015**, 3066.

[58] C. Wellm, M. Rams, T. Neumann, M. Ceglarska, C. Näther, *Cryst. Growth Des.* **2018**, *18*, 3117.

[59] S. Wöhlert, Z. Tomkowicz, M. Rams, S. G. Ebbinghaus, L. Fink, M. U. Schmidt, C. Näther, *Inorg. Chem.* **2014**, *53*, 8298.

[60] P. Horcajada, R. Gref, T. Baati, P. K. Allan, G. Maurin, P. Couvreur, G. Férey, R. E. Morris, C. Serre, *Chem. Rev.* **2012**, *112*, 1232.

[61] S. Suckert, M. Rams, M. M. Rams, C. Näther, *Inorg. Chem.* **2017**, *56*, 8007.

[62] R. Hilfiker, *Polymorphism in the Pharmaceutical Industry*, 1 ed., Wiley-VCH Verlag GmbH & Co. KGaA, Weinheim, **2006**.

[63] A. I. Kitaigorodski, *Organic Chemical Crystallography*, Consultants Bureau, New York, **1961**.

[64] H. G. Brittain, *Polymorphism in Pharmaceutical Solids*, 1 ed., Vol. 23, Marcel Dekker, **1999**.

[65] K. Robinson, G. V. Gibbs, P. H. Ribbe, *Science* **1971**, *172*, 567.

[66] J. Werner, M. Rams, Z. Tomkowicz, C. Näther, *Dalton Trans.* **2014**, *43*, 17333.

[67] R. A. Bailey, S. L. Kozak, T. W. Michelsen, W. N. Mills, *Coord. Chem. Rev.* **1971**, *6*, 407.

[68] M. E. Fisher, *Philos. Mag.* **1962**, *7*, 1731.

[69] H. A. Groenendijk, H. W. J. Blöte, A. J. van Duyneveldt, R. M. Gaura, C. P. Landee, R. D. Willett, *Phys. B* **1981**, *106*, 47.

[70] G. M. Sheldrick, *SHELXS-97*, University of Göttingen, Göttingen, Germany, **1997**.

[71] G. M. Sheldrick, *Acta Crystallogr., Sect. A* **2015**, *71*, 3.

[72] G. M. Sheldrick, *Acta Crystallogr., Sect. C* **2015**, *71*, 3.

[73] Stoe&Cie, *X-AREA* (Version 1.44). STOE & CIE GmbH, Darmstadt, Germany, **2008**.

Received: July 25, 2018

*A. Jochim, M. Ceglarska, M. Rams, C. Näther** **1–12**

Synthesis, Crystal Structures, and Properties of Ni(NCS)$_2$-4-methoxypyridine Coordination Compounds